Surface & Coatings Technology 404 (2020) 126486

Contents lists available at ScienceDirect

Surface & Coatings Technology

journal homepage: www.elsevier.com/locate/surfcoat

Biofunctionalization of PEO coatings on titanium implants with inorganic and organic substances

Evgeny Parfenov[a,*], Lyudmila Parfenova[b], Veta Mukaeva[a], Ruzil Farrakhov[a], Andrey Stotskiy[a], Arseniy Raab[a], Ksenia Danilko[c], Nagumothu Rameshbabu[d], Ruslan Valiev[a]

[a] Ufa State Aviation Technical University, Ufa, Russia
[b] Institute of Petrochemistry and Catalysis of Russian Academy of Sciences, Russia
[c] Bashkir State Medical University, Ufa, Russia
[d] National Institute of Technology, Tiruchirappalli, India

ARTICLE INFO

Keywords:
Titanium implants
Plasma electrolytic oxidation
Microarc oxidation
Biocompatible coatings
Hydroxyapatite
RGD-peptide

ABSTRACT

The paper concerns a choice in the biofunctionalization of the coatings produced by plasma electrolytic oxidation: either with inorganic components by introducing Ca-, P- containing compounds into the coating (primarily hydroxyapatite), or with integrin-active organic components (primarily RGD peptides). The following coatings were analyzed: E1 – titania PEO coating, E2 – titania and Ca-, P containing PEO coating, E1 + RGD – titania PEO coating modified with integrin-active RGD (arginine-glycine-aspartic acid) tripeptide sequence anchored to the surface with a bisphosphonate linker. In terms of wear resistance, electrochemical corrosion behavior, and interaction with osteoblast-like cells, coating E1 + RGD seems to be the most promising for the titanium implants.

1. Introduction

Titanium is widely used in traumatology and orthopedics as a material suitable for permanent implants; Ti is a bioinert, non-magnetic, and non-toxic material that exhibits high biocompatibility, high corrosion resistance, low thermal conductivity, small linear expansion coefficient, and relatively low specific weight [1]. Under a long-term exposure, titanium implant releases metal ions which penetrate surrounding tissue in the corrosive environment of a human body, especially under the influence of mechanical loads; protective coatings can reduce this effect [2]. Recently, plasma electrolytic oxidation (PEO), alternatively called microarc oxidation (MAO), has attracted great interest because of its advantages compared to other methods [3–5]. PEO coatings contain stable oxides (rutile and anatase) and have good adhesion to the substrate [6]. The PEO coatings on Ti can be obtained with a different ratio of rutile and anatase, e.g. by variation of the current density and treatment time; it is generally acknowledged that anatase contributes more to the titania coating bio-compatibility, and rutile + anatase coatings with the anatase content higher than 50% appear to be the most promising [7–10]. The pore size of the PEO-coating ranges from 0.1 to 10 μm; high surface area of the PEO coating promotes osteoblast attachment on the implant surface [11]. The mesh of pores which are developed in the coating due to the action of the microdischarges forms a fractal structure, with pores enlarging to the surface [12]; such morphology provides a gradual change of mechanical properties from the implant metal to the bone; this increases biomechanical compatibility as well.

Two biofunctionalization trends are clearly seen in the current research into the PEO coatings: this is a modification with either inorganic or organic components [13,14]. For both approaches, the PEO technology appears to be suitable, (i) by incorporation of the inorganic electrolyte components and their transformation in the microdischarge plasma [15], and/or (ii) by the introduction of the organic substances into the titania coating pores [16].

Within the first approach, it was shown that inorganic components containing calcium and phosphorus improve the biocompatibility of the oxide coatings compared to bare Ti substrate [17–19]. It was shown that by immersion of the Ca-, P- containing PEO coatings into the simulated body fluid (SBF), the hydroxyapatite (HA), which is the main crystalline component of a human bone, is formed [9,20]. This effect can be enhanced by further post-processing, e.g. by hydrothermal or chemical treatments [21,22]. Varying the electric regimes of the PEO helps to incorporate the anions and cations of the electrolyte into the coating; this generates in situ Ca-, P- containing bioactive crystalline phases within the coating: hydroxyapatite, tricalcium phosphate, perovskite [23,24]. Using duplex methods of PEO coupled with

* Corresponding author.
E-mail address: evparfenov@mail.ru (E. Parfenov).

https://doi.org/10.1016/j.surfcoat.2020.126486
Received 14 June 2020; Received in revised form 28 August 2020; Accepted 6 October 2020
Available online 10 October 2020

electrophoretic deposition (EPD) helps to incorporate hydroxyapatite, silver, and other nanoparticles into the coating [25–28]. The current trend includes also introduction of various functional elements into the HA-PEO coatings to improve their biocompatibility: Ag, F, and Y for antimicrobial activity [4,29–31], Zn, Si and Mg for triggering the HA formation [13,32]. However, despite the great number of published papers that investigate HA containing PEO coatings, there is no answer, to the current knowledge of the authors, whether or not Ca-, P- containing PEO coating provides better cell response compared to titania only PEO coating. Many authors acknowledge the benefits of the PEO coating over the Ti substrate, but among the various compared inorganic PEO coatings, no significant differences in the cell response have been reported [3,14,33].

Within the second approach, organic modifiers for the PEO coatings include polytetrafluoroethylene [34,35], polyethylene glycol [36], oligopeptides [37,38] and proteins [39], polysaccharides [16,40,41], antimicrobial peptides [42] and antibiotics [14,43]. For the deposition of the organic top-coat, complex plasma polymerization and UV-grafting equipment can be required [16]. One of the important options in this approach is the application of the motifs of extracellular matrix proteins, for example, RGD (arginine-glycine-aspartic acid); this tripeptide fragment promotes signaling with the cells and results in their attachment on the surface [44]. Unlike other mentioned above organic substances, RGD has a small acting concentration in the order of 10^{-4}…10^{-3} M [37,38,45,46]; therefore, the formed organic monolayer cannot be directly detected by SEM and EDS, and reliable indicators of the successful RGD modification of the porous PEO coating must be elaborated, and appropriate methods must be formulated. As shown earlier in our research, the introduction of the RGD tripeptide via an appropriate linker onto the PEO coating increases the cell proliferation on the examples of fibroblasts, mesenchymal stem cells and osteoblast-like cells [37,38]. It was shown that the RGD-derivatives, when attached to the PEO oxide layer, alter the electrochemical properties by increasing the corrosion currents and shifting the corrosion potential to less noble values; however, further studies of this effect are required. Moreover, in-depth XPS characterization is needed to support the mechanism of the anchoring the RGD derivatives on the PEO surface.

Therefore, it is not clear so far, which approach, Ca-, P- inorganic modification, or RGD organic modification, appears to be more beneficial for the PEO technology development towards the increase in the biocompatibility of the Ti implants. Consequently, this work aims at a comparison of the PEO coatings modified by inorganic Ca-, P- and organic RGD substances in terms of their mechanical, physicochemical, electrochemical, and biological properties.

2. Experimental

2.1. PEO and RGD coatings

Commercially pure titanium (Cp-Ti) was used as the substrate material for the study. The chemical composition of the Cp-Ti is (wt%): Fe – 0.3, C – 0.1, O – 0.25, N – 0.03; H – 0.015, Ti – balance. To use a 24-well culture plate for the in vitro tests, the samples were disk-shaped with a diameter of 10 mm and a thickness of 0.5 mm, and surface roughness of Ra $\leq$ 0.15 μm.

The coating experiments were performed using the automated installation for plasma electrolytic oxidation described elsewhere [37]. During the PEO, the electrolyte was homogenized with a magnetic stirrer. The sample holder was made of 1 mm diameter Cp-Ti wire wrapped around the sample; the holder was also oxidized. Two electrolytes were used to produce titania-only PEO coating labeled as E1, and Ca-, P- containing titania coating labeled as E2. The PEO process details are summarized in Table 1.

The RGD-derivative of (3-{[3-(2,5-dioxo-2,5-dihydro-1H-pyrrol-1-yl)propanoyl]amino}-1-hydroxypropane-1,1-diyl)-bis-(phosphonic acid) (RGDC-BMPS-β) was synthesized according to the method described elsewhere [37,38]. This compound which structure is shown in Fig. 1 was used as the most effective one, according to the previous research. In order to produce the RGD-containing titania coating E1 + RGD, the samples E1 were put into 10^{-3} M water solution of the RGD-derivative; after 1 h of the soaking, the samples were dried on the air.

2.2. Surface characterization

The coating morphology was studied using the Zeiss Gemini-300 scanning electron microscope (SEM) equipped with energy dispersive spectroscopy (EDS) attachment. The phase composition of the surface layer was characterized by X-ray diffractometer Rigaku Ultima IV in Cu Kα radiation at 40 kV and 40 mA using 0.02 deg. step scan with 2 s exposure, from 20 to 80 degrees 2θ. Further, the XRD spectra were processed using Philips X'Pert Highscore Plus software; the quantitative analysis was made with a SemiQuant procedure. The average pore size and porosity (percentage of surface area occupied by pores) were determined from the SEM images using ImageJ software following ASTM E112-10. The coating thickness was measured with an eddy current thickness gauge Defelsko Positector 6000, and also verified with the coating cross-section images. An optical Taylor Hobson Talysurf CCI profilometer was used to study the surface topography. The adhesion strength test was carried out on a Revetest instrument (CSM Instruments, Switzerland) using a spherical Rockwell C diamond indenter with a tip radius of 200 μm and an optical microscope as an attachment for observing the scratch path. Scratch test was carried under the progressive load (1 – 20N) with a loading rate of 9.5 N/min over a scratch length of 5 mm at a scratch speed of 2.5 mm/min. The scratch track images provided the critical loads (Lc) corresponding to the bright appearance of the metallic substrate, indicating the coating failure. Also, the coefficient of friction was estimated from the dependencies of the frictional force vs. load.

Because of the low work concentration of the RGD containing solution (10^{-3} M), the mentioned above methods are unable to detect whether or not the RGD peptide was linked to the PEO coating. Therefore, XPS spectra were obtained using a JEOL JPS 9010MX spectrometer equipped with an (Mg Kα) X-ray source. The pressure in the analytical chamber during spectral acquisition was less than $7{\cdot}10^{-8}$ Pa. The spectra were collected from 0 to 1100 eV with a pass energy of 50 eV and 0.5 eV step. JEOL SpecSurf software was used to determine peak areas, to calculate the elemental compositions from the peaks, and to fit peaks the high-resolution spectra.

The electrochemical tests were carried out in Ringer's solution at room temperature using P-5× (Elins, Russia) electrochemical system. Open circuit potential (OCP) measurements, electrochemical impedance spectroscopy (EIS) from 100 kHz to 1 mHz with the magnitude of 10 mV around the OCP, and potentiodynamic polarization (PDP) –350/+350 mV vs. OCP at a rate of 0.25 mV/s were performed. A silver chloride electrode filled with 3.5 M KCl was used as a reference electrode. The counter electrode was a platinum rod. The PDP results were processed using the Tafel method. The polarization resistance R_p was calculated from the slope of the polarization curve at ± 10 mV around the free corrosion potential. The EIS results were analyzed using ZView software from Scribner Associates [47].

To ensure reproducibility, 3 identical samples were tested, and the results were averaged.

2.3. In vitro tests

The E1 or E2 coated Ti samples were ultrasonically cleaned for 10 min in 95% ethanol and finally washed with deionized water, dried on air, and sterilized by autoclaving at 134 °C. This temperature does not affect the PEO coatings. In order to deposit the organic pore filler, the samples E1 were put into a Petri dish with 10^{-3} M water solution of the RGD-derivative, which was preliminarily sterilized by filtration

Table 1
Sample codes with the corresponding PEO process conditions.

Sample code	Electrolyte composition	Positive pulse		Negative pulse		Frequency (Hz)	Temperature (°C)	Duration (min.)
		Voltage (V)	Duty cycle (%)	Voltage (V)	Duty cycle (%)			
E1	20 g/l $Na_3PO_4{\cdot}12\ H_2O$	470	51	40	26	300	20 ± 1	5
E2	20 g/l $Na_3PO_4{\cdot}12\ H_2O$ + 25 g/l Ca $(CH_3COO)_2$							

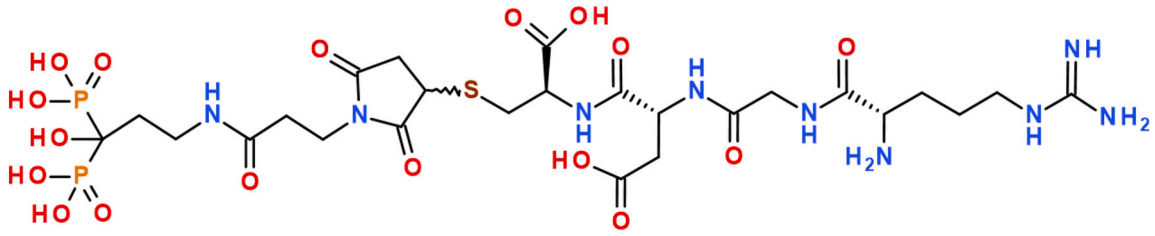

Fig. 1. Structure of RGD derivative used for the functionalization of the PEO coating E1.

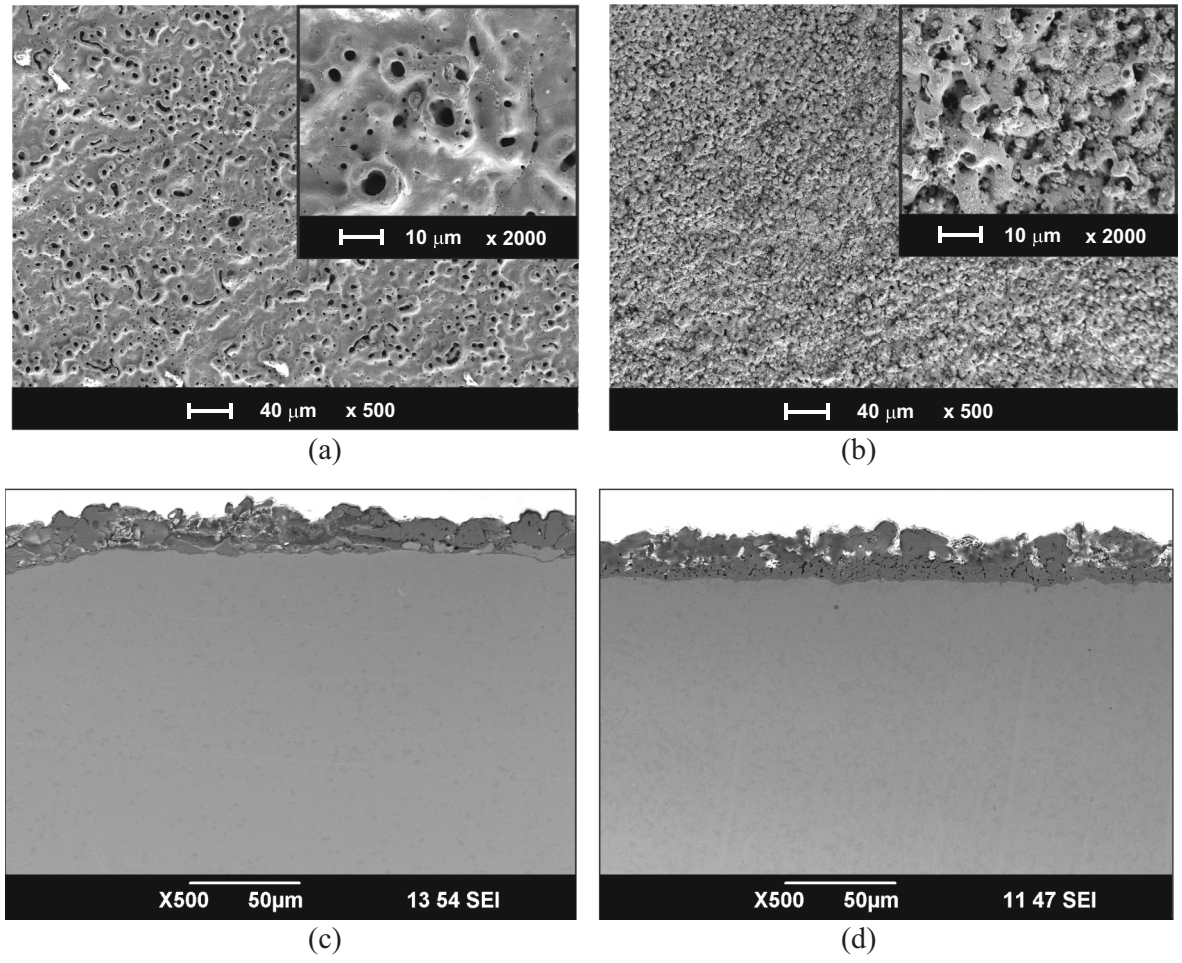

Fig. 2. SEM images of the top view (a, b) and cross-section (c, d) of the PEO coatings E1 (a, c) and E2 (b, d) on Ti.

with CA0.22 μm filter. After 1 h of the soaking, the samples were dried on the air in a laminar box. Then, all the samples were put into polystyrene 24-well tissue culture plate.

Human osteosarcoma cells (MG-63) were obtained from Russian cellular collection, Institute of Cytology RAS (Russia). The cells were cultured in Dulbecco's modified Eagle's medium (DMEM) (Sigma) containing 10% fetal bovine serum (FBS) (BioWest) and gentamicin 100 mg per ml, in 25-cm^2 culture flasks (SPL life Sciences) in a humidified 5 vol% CO_2 atmosphere at 37 °C. The medium was changed twice a week. After reaching a monolayer, the cells were detached using 0.25% trypsin solution (PANECO) and counted using automated cell counter TC20 (BioRad).

The cell suspension was placed into each well of the plate with the samples (0.8 ml containing $20{\cdot}10^3$ cells). The cells in the wells with E1

samples were treated as a control. The culture plates were incubated for 7 days in the standard conditions (37 °C, 5 vol% CO_2). The culture plate itself (polystyrene) was used as a blank.

The cell proliferation on the samples was determined by EZ4U assay (Biomedica), a modification of the MTT test, which evaluates the cell metabolic activity being proportional to the number of the living cells. Three samples of each type were transferred after the incubation into another 24-well plate with 0.8 ml of fresh DMEM medium. Then 80 μl of activated EZ4U solution was added to every well and incubated at 37 °C, 5 vol% CO_2 for 3.5 h. Optical absorbance was measured using a microplate reader (Spark10M, Tecan) at 450 nm with a reference wavelength of 620 nm. The optical density was calculated as

$$\text{Optimal density with respect to control}\,(\%) = \frac{(a - a_{blank})}{(A - a_{blank})}100\%, \quad (1)$$

where a – absorbance of the test sample at 450 nm minus absorbance at 620 nm;

A – absorbance of the control sample at 450 nm minus absorbance at 620 nm;

a_{blank} – the absorbance of the blank solution of DMEM with no cells at 450 nm and 620 nm.

The mean value and the standard deviation for four measurements of the optical density were calculated with respect to the control. The data were analyzed using one way ANOVA and Bonferroni's multiple comparisons test (GraphPad Prism, v.6.01) at a significance level of $p < 0.05$.

3. Results and discussion

3.1. Characterization of titania and Ca-, P- containing PEO coatings

Fig. 2 shows the top view and cross-section SEM images of the samples with the PEO coatings obtained in electrolytes E1 and E2. The coating E1 + RGD has no morphological differences from E1 because the work concentration of the RGD water solution is quite low. The SEM images obtained for the E1 + RGD coatings appear the same as in Fig. 2a. Parameters in Table 2 describe the morphology of the coatings, which have a porous structure typical for the PEO; this morphology is a result of the microdischarge action that melts the titania which then resolidifies due to the surrounding electrolyte cooling effect. The unique morphology of the PEO coating with a well-developed network of pores is similar to the surface of the human bone; these coatings can be considered as biomimetic [48].

As follows from Fig. 2 and Table 2, morphological features of the coatings are different for samples E1 and E2. A comparison of the cross-sections shows that the E2 coating is thicker; both the surface open porosity and the inner layer porosity is higher for the E2 coating. The introduction of calcium acetate into the electrolyte significantly changes the morphology of the E2 coating. Its thickness, roughness, and porosity increased, and the average pore size decreased. The higher roughness of E2 coating increases the surface area available for the cell attachment.

As follows from the EDS analysis, the E1 coating contains Ti and O, and also a small amount of the electrolyte species – Na and P (Table 3). The E2 coating also features significant amounts of Ca and P. As follows from the EDS mapping (Fig. 3), the titanium mainly appears in the pore sites, probably, this is the effect of the substrate. Ca-, P- compounds appear around the pores. This suggests that they are incorporated into the coating structure as micro-particles seen in Fig. 2b at higher magnification.

The X-ray diffractometry method showed that the phase composition of the coatings substantially depends on the components of the electrolyte. Both E1 and E2 coatings contain rutile and anatase phases (Fig. 4). The combination of these compounds has a positive effect on the survival rate of living cells [3]. In E1 coating, anatase makes up a larger proportion (Table 4), which favorably affects biocompatibility [49]. For E2 coating, titania constitutes about 13% of the crystalline phase, and the rutile content is higher than that of the anatase. This can be explained by the fact that the coating E2 is much thicker than E1. The formation of the rutile, which is a higher temperature phase, requires more energy than the formation of the anatase. When the coating is thin, the PEO microdischarges are small, and they have relatively low power; as a result, anatase is predominantly formed under such conditions. During the breakdown of a thicker coating, the powerful microdischarges contribute to the formation of the rutile. In addition to the rutile and anatase, the E2 coating contains bioactive substances of perovskite $CaTiO_3$, hydroxyapatite $Ca_{10}(PO_4)_6(OH)_2$. Also, the X-ray diffractogram exhibits a wide peak of the amorphous calcium phosphates in the range of 2θ from 25° to 45°, and amorphous calcium phosphates make up a significant proportion of the coating which is consistent with the literature [19,37].

Analysis of the mechanical performance of the coatings assessed by the scratch test showed that E1 coating has better adhesion strength compared to E2 coating. As follows from Fig. 5, the destruction of E1 coating occurs at critical load Lc = 11.1 ± 0.9 N when the continuous bright appearance of the titanium substrate can be seen; the Lc for the E2 coating is 8.6 ± 0.7 N. This result is consistent with the data presented elsewhere [50]. For E1 coating the frictional force randomly deviates from the growing trend line with the same variance for the coating and the substrate. However, for E2 coating the deviation is smaller at lower loads suggesting that the Ca-, P- phases being softer than rutile and anatase [51], provide some lubrication; therefore, the coefficient of friction is smaller for this coating (Table 2). This area on the load curve also appears at the loads larger than Lc because the partly damaged coating still offers the lubrication and support for the spherical indenter tip. Therefore, the thinner and harder E1 coating has a lower likelihood of chipping under bending and twisting loads during the implantation; moreover, the porous morphology will likely be less likely destroyed for E1 coating, as it does not provide the lubrication due to the damage of the calcium phosphates.

3.2. XPS investigation of the PEO-inorganic and PEO-organic coatings

Fig. 6 shows the XPS survey spectra of the samples under investigation. The spectra parameters are presented in Table 5, and the peak deconvolutions are shown in the Supplementary material. The sensitivity of this method allowed us to determine both inorganic and organic components in the coating. The spectra contain the peaks of C1s, Ti2p, O1s, P2p, Ca2p, and N1s. C1s hydrocarbon maximum (284.8 eV) appears due to the adsorption of ubiquitous species from the air and electrolyte. Sample E1 provides the spectra typical to PEO-modified Ti [15]. Deconvolution of the Ti2p spectra with Voigt functions uncovers the peaks at 264.5 and 458.46 eV, attributed to $2p_{1/2}$ and $2p_{3/2}$ components of Ti^{4+} in Ti- O bonds of TiO_2 layer [52], as

Table 2
Surface properties of PEO treated samples E1 and E2.

Sample code	h (μm)	Rz (μm)	Ra (μm)	Porosity (%)	Average pore size (μm)	Critical load, N	Coefficient of friction (coating vs. Rockwell diamond tip)
E1	18.6 ± 4.8	14.8 ± 2.7	2.1 ± 0.4	6.8 ± 0.4	0.82 ± 0.17	11.1 ± 0.9	0.20 ± 0.1
E2	23.2 ± 5.2	19.3 ± 2.3	3.1 ± 0.5	14.5 ± 0.4	0.77 ± 0.16	8.6 ± 0.7	0.17 ± 0.1

Table 3
The elemental composition of samples E1 and E2 obtained by EDS.

Sample code	Elements (wt%)					
	Ti	O	P	Na	Ca	C
E1	46.63 ± 5.63	45.80 ± 3.93	5.72 ± 1.26	1.83 ± 0.56	–	–
E2	15.4 ± 2.78	42.00 ± 1.90	10.4 ± 0.87	1.11 ± 0.24	27.98 ± 5.73	3.08 ± 0.83

shown in Fig. S.1. The presence of additional peaks at 462.8 and 456.3 indicates the possible formation of Ti_2O_3 admixture in the coating [53–55]. However, a crystalline form of this compound has not been found by XRD. The spectrum of O1s exhibits three components at 530.6 eV, 531.8 eV and 532.2 eV, related to Ti—O, Ti-OH groups and adsorbed H_2O, correspondingly [56–58]. The XPS N1s peak at 396.7 eV is indicative of a typical atmospheric contamination.

The inorganic Ca—P additive in E2 coating significantly changes the spectral response (Fig. 6). The intensity of titanium Ti2p peak is very small, whereas the peaks of calcium (Ca1s, Ca2s, and Ca2p) and phosphorus (P2p) are noticeably higher compared to the sample E1. Two peaks of Ca2p with binding energies of 347.4 eV for $Ca2p_{3/2}$ and 350.9 eV for $Ca2p_{1/2}$, as follows from Fig. S.2, correspond to the presence of $Ca_3(PO_4)_2$ and $Ca_{10}(PO_4)_6(OH)_2$ in the coating [58–61]. The P2p spectrum is a doublet with $2p_{1/2}$ and $2p_{3/2}$ components with binding energies of 133.5 and 134.4 eV (Fig. S.2); this indicates the appearance of the phosphates in the coating [58,61–63]. Therefore, the coating outer layer consists mainly of calcium phosphate compounds (HA, perovskite) that interrupt the supply of titanium for the production of titanium oxide during the growth of the coating [64]. With the increase of the coating thickness, the population of the plasma microdischarges becomes sparse, and the electrochemical and electrophoretic processes begin to prevail on the surface of the oxide layer [65].

After the RGD modification, the most notable differences between E1 and E1 + RGD samples can be seen in C1s, O1s, P2p, N1s, and S2p spectral lines. For the E1 + RGD sample, the C1s signal appears to be substantially increased and asymmetrically broadened. The presence of a dominant ether/amine peak (285.9 eV, C–NH_2, C—O), amide N–C=O, and C=O (288.6 eV) groups [66,67] indicate the formation of the RGD layer. N1s signal decreases in magnitude and shifts to 400.4 eV due to the RGD appearance on the surface. This signal could be attributed to amine and amide species [66,68]. These results show that the organic components penetrate the PEO coating and remain in its pores.

The O1s line of the E1 + RGD sample can be deconvoluted with three functions. The signal at 530.6 eV is attributed to the Ti—O bond in the initial TiO_2, whereas the increase in the component intensity at 531.8 eV may be due to the appearance of Ti-O-P and P=O groups [57,69,70]. The component at 533.1 eV could be ascribed to P–OH sites [71–73]. The ratio of the peak intensities at 531.8 eV and 533.1 eV is 2.8, which is consistent with the covalent bonding of the phosphonic acids to the oxidized metal surface by a transformation of the end P–OH groups to P–O–M sites. The binding of one P—O group to the oxide layer should lead to the signal intensities ratio (531.8 eV/533.1 eV) as 2:1. The larger value obtained in our case implies that some phosphonate fragments have two P-O-M interactions and no free P-OH groups. This type of anchoring could be the reason for the relative stability of self-assembled monolayers [74]. This is also consistent with the tendency of phosphonates to bidentate coordination to the TiO_2 surface [75]. Moreover, bisphosphonates are tended to form multilayers that resist desorption even in the presence of phosphate ions and determine the organic coating stability on the TiO_2 surface [76]. Such coating organization predetermines both bidentate and monodentate binding when the part of P-OH groups remain unbound, as follows from the O1s spectra. The multilayer organization of the bisphosphonates is supported by the P2p spectrum. With the appearance of RGD-modified bisphosphonate molecules in the E1 sample, signal growth is observed. This signal is the sum of two major doublets with the main peaks $2p_{3/2}$ at 132.7 and 133.9 eV, as well as the two minor components at 135.4 and 136.2, which can correspond to different variants of bisphosphonate group coordination to the TiO_2 coating [70,73].

3.3. Electrochemical behavior of the PEO-inorganic and PEO-organic coatings

Fig. 7 shows potentiodynamic polarization curves for samples E1, E2, E1 + RGD, and an uncoated sample. The corrosion parameters are presented in Table 6. As can be seen from the E_{corr} values, PEO treatment in electrolytes E1, E2 leads to the surface passivation because higher E_{corr} is observed. The introduction of the RGD organic compound depassivates the surface and shifts E_{corr} down, but higher the

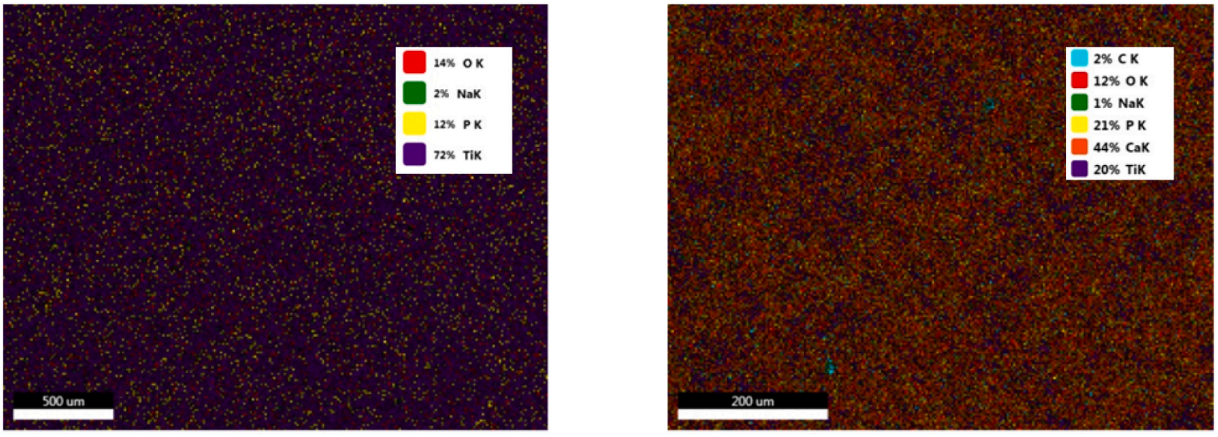

Fig. 3. EDX mapping of the elements constituting the PEO coatings E1 (a) and E2 (b) on Ti; the legends show the color and the percentage of the pixels associated with the detected elements. (For interpretation of the references to color in this figure legend, the reader is referred to the web version of this article.)

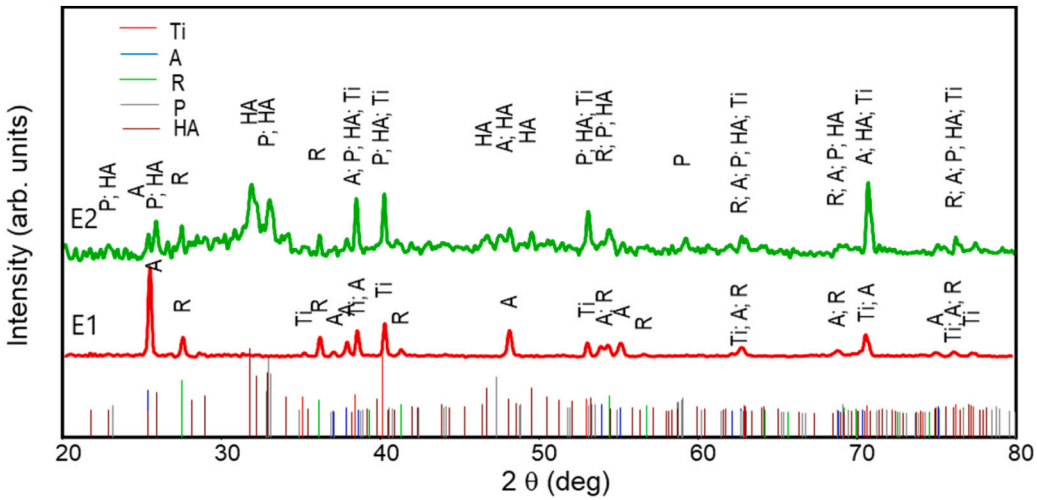

Fig. 4. X-ray diffractograms of the PEO coatings E1 and E2 on Ti (abbreviations and PDF reference codes: Ti – titanium substrate (00-044-1294), A – anatase (01-084-1286), R – rutile (01-072-1148), P – perovskite $CaTiO_3$ (01-081-0562), HA – hydroxyapatite $Ca_{10}(PO_4)_6(OH)_2$) (01-086-0740).

Table 4
XRD semi-quantitative estimation of the crystalline phase content of the PEO coatings E1 and E2.

Sample code	Rutile	Anatase	Perovskite	Hydroxyapatite
E1	25.8 ± 3.2	74.2 ± 4.1	–	–
E2	10.2 ± 1.3	3.5 ± 0.6	22.5 ± 2.6	63.8 ± 4.6

value for the substrate. Also, the PEO coating reduces the corrosion current i_{corr} by an order of magnitude compared to the uncoated sample; the i_{corr} values for samples E1 and E2 differ slightly, within the experimental tolerance interval. The introduction of the RGD increases the i_{corr} up to the value of the Ti substrate. This current increase can be due to the action of the RGD compounds which adsorb in the pores of the coating down to the substrate; as a result, the surface of the coating becomes more active and more conductive. Nevertheless, the introduction of the RGD peptides should not promote excessive corrosion damage to the coating, because the E_{corr} for E1 + RGD coating is still nobler than that of the substrate, and its corrosion current values appear within the tolerance interval with those of the titanium substrate that is generally considered as corrosion resistant. The polarization resistance R_p data are in good agreement with the values of the corrosion current. The samples E1 and E2 have the highest polarization resistance. The R_p value of E1 + RGD sample is an order of magnitude less than that of E1 and E2. The uncoated sample has the lowest polarization resistance.

The electrochemical impedance spectra are shown in Fig. 8 as complex and Bode plots; they have significant differences among the samples. The uncoated Ti sample has a thin natural oxide layer. Its impedance spectrum shows one time constant; therefore, it can be approximated with a Randles CPE containing equivalent circuit which describes typical for a defect-free thin film one-step corrosion reaction without diffusion (Fig. 9a). The complex plots of E1 and E2 spectra

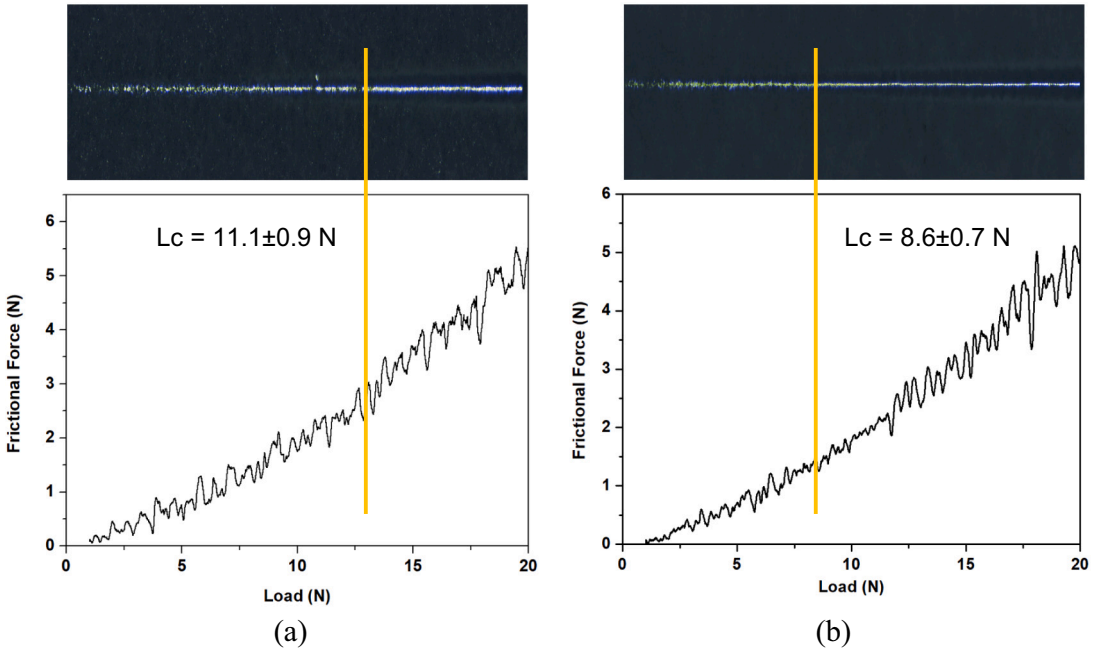

Fig. 5. Frictional force vs. load and wear tracks of the scratch tests of E1 (a) and E2 (b) PEO coatings on titanium; the critical loads (Lc) corresponding to the bright appearance of the metallic substrate due to the coating failure are shown with lines.

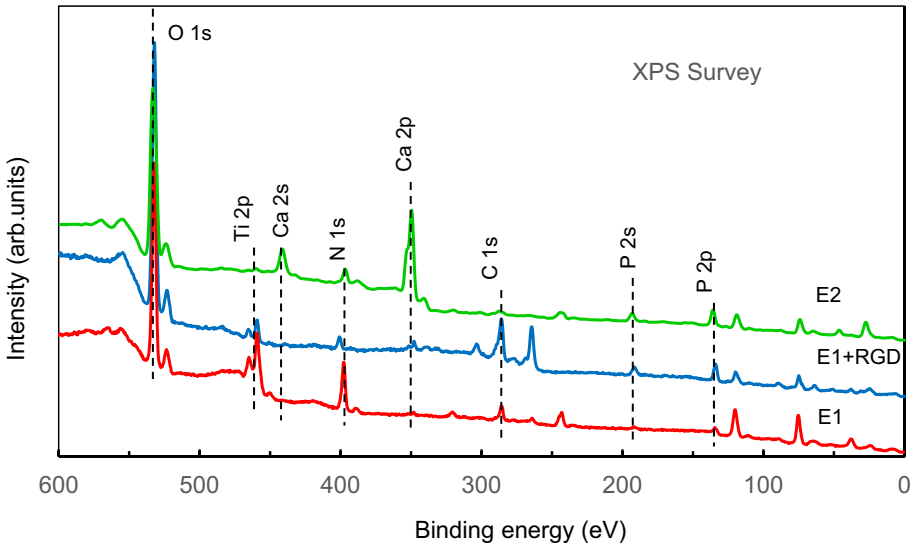

Fig. 6. XPS survey spectra of the PEO coatings E1, E1 + RGD and E2.

Table 5
XPS analysis of the PEO coatings E1, E2 and E1 + RGD.

Sample code	XPS atomic composition (at.%)							
	N1s	P2p	C1s	O1s	Ti2p	S2p	Ca2s	Ca2p
E1	13.79	1.59	3.39	64.12	16.22	0.00	0.00	0.90
E2	2.60	3.91	1.56	54.38	0.78	0.00	7.78	29.00
E1 + RGD	2.75	4.16	13.74	73.71	5.53	0.11	0.00	0.00

show a linear increase in the impedance at the lowest frequencies; this indicates a presence of the Warburg impedance, which reflects the diffusion processes occurring in the pores of the coatings. The spectra also show one time constant at higher frequencies; therefore, they can be approximated with a Randles circuit for a system with diffusion (Fig. 9b). The complex plot for the E1 + RGD sample contains two time constants; this indicates the presence of two layers in the coating. This spectrum was approximated with a ladder circuit (Fig. 9c). The difference between the E1 and E1 + RGD electrochemical impedance spectra confirms the presence of the organic RGD compound in the PEO coating. This difference appears at the lowest frequencies, therefore, in the thinnest part of the coating – barrier layer; the diffusion-controlled process described by Wo1 for the titania PEO coating E1 is transformed into a kinetically controlled process described by R3-CPE2. This effect reduces the low-frequency impedance of the coating, and it is consistent with the polarization resistance estimates.

Table 7 presents the parameter values for the equivalent circuits. The electrolyte resistance was estimated as R1 = 41.1 ± 14.0 Ω cm^2 for all the samples. In the Randles circuits (Fig. 9a, b), R2 is the charge transfer resistance. The uncoated sample has the highest value of R2 since the natural oxide layer has a defect-free structure. The samples after the PEO have porous coating; consequently, R2 decreases. The

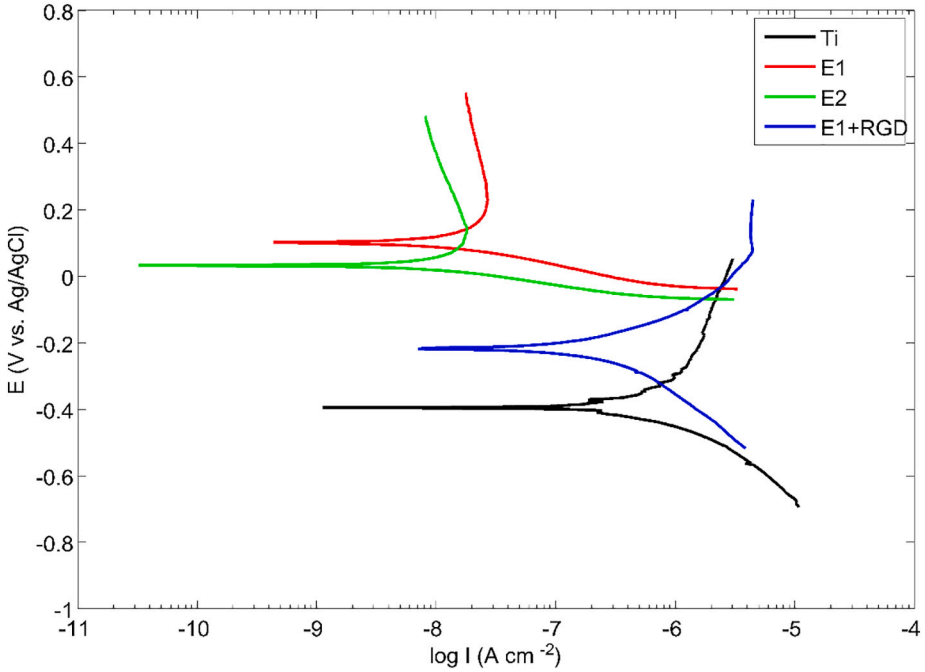

Fig. 7. Polarization curves for the corrosion tests of Ti substrate and the PEO coatings E1, E1 + RGD and E2 in Ringer's solution.

Table 6
Corrosion properties of the PEO coatings E1, E2 and E1 + RGD in Ringer's solution.

Sample code	Ti	E1	E2	E1 + RGD
E_{corr} (V vs. Ag/AgCl)	−0.395 ± 0.05	0.1024 ± 0.005	0.0331 ± 0.029	−0.218 ± 0,001
i_{corr} (A·cm^{-2})	$1.57{\cdot}10^{-7}$ ± $0.8{\cdot}10^{-8}$	$9.45{\cdot}10^{-9}$ ± $0.8{\cdot}10^{-9}$	$7.67{\cdot}10^{-9}$ ± $1.2{\cdot}10^{-9}$	$2.16{\cdot}10^{-7}$ ± $1.12{\cdot}10^{-7}$
Rp (Ω·cm^2)	$8.08{\cdot}10^{4}$ ± $0.4{\cdot}10^{4}$	$1.54{\cdot}10^{6}$ ± $0.7{\cdot}10^{5}$	$1.79{\cdot}10^{6}$ ± $2.32{\cdot}10^{5}$	$1.73{\cdot}10^{5}$ ± $0,8{\cdot}10^{4}$

CPE-Q parameter of the constant phase elements in all the equivalent circuits can be considered as an estimate of the distributed capacitance of the double layer which reciprocal is correlated with the coating thickness $h{\sim}\frac{1}{CPE-Q}$. A substantial CPE1-Q value indicates a thin oxide layer in the uncoated sample. For E1 and E2 samples, the CPE1-Q value is an order of magnitude lower; the values of CPE1-Q for samples E1 and E1 + RGD are approximately the same since the coating thicknesses have small variation for the PEO technology. The coating thickness of the E2 sample is twice as higher than that of E1; therefore, the CPE1-Q value for the E2 sample is twice as lower than that of E1. The CPE-n value shows a degree of the equivalent capacitance "non-ideality", with CPE-n = 1 for an ideal capacitor. Therefore, the uncoated sample has higher CPE-n than E1. Also, E2 has this value closer to the uncoated sample; therefore, R2 in this case is higher than that for E1, showing less developed porosity in the coating, because of Ca-, P-species incorporation as micro-particles. The Warburg impedance parameters Wo-R (equivalent resistance) and the Wo-T (time constant), describing the diffusion, differ for samples E1 and E2. The porosity of E1 coating is approximately two times lower compared to E2 coating; this leads to the difficulties in the diffusion processes and results in larger values of the Wo-R and Wo-T parameters. For the E1 + RGD sample, the elements R2 and CPE1 in the ladder circuit (Fig. 9c) correspond to the equivalent resistance and capacitance of the PEO coating, and the pair R3 – CPE2 describes the charge transfer through the coating inner barrier layer; R3 is the charge transfer resistance, and CPE2 the "non-ideal" capacitance of the double layer. Since the inner barrier layer is more compact than the outer PEO coating layer, its resistance R3 is significantly larger than R2. Moreover, the higher value of CPE2-Q compared to CPE1-Q (having almost the same CPE-n) shows that this assignment of the equivalent circuit elements is correct.

Therefore, the results of PDP and EIS tests demonstrate that the introduction of the organic RGD layer over an inorganic porous PEO coating depassivates the surface and change the dominant process governing the charge transfer in the barrier layer during the corrosion in Ringer's solution, from diffusion to kinetic control.

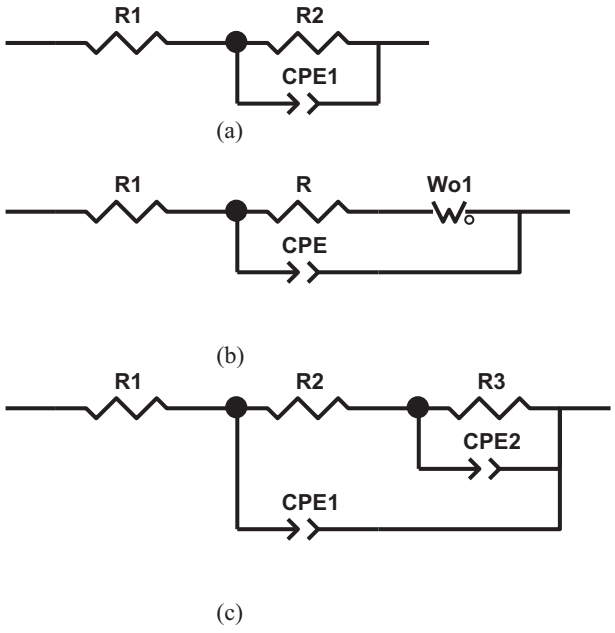

Fig. 9. Equivalent circuits employed for the EIS results fitting: (a) Ti substrate; (b) coatings E1 and E2; (c) coating E1 + RGD.

3.4. *In vitro performance of the PEO coatings biofunctionalized with inorganic and organic compounds*

Fig. 10 presents the results of in vitro tests. There is a decrease in

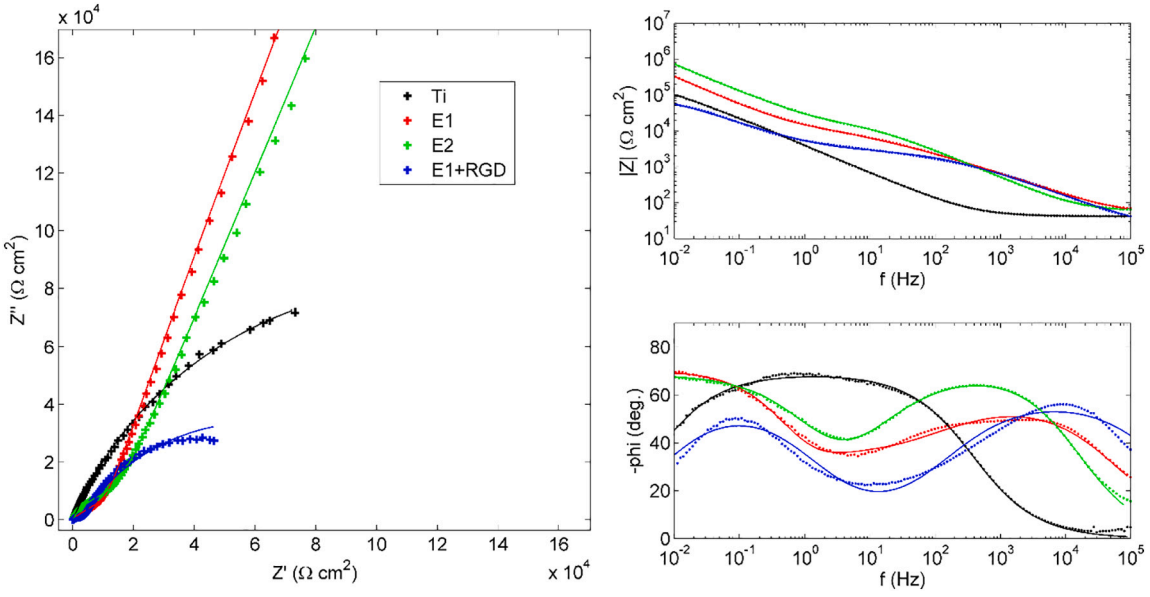

Fig. 8. Electrochemical impedance spectra of Ti substrate and the PEO coatings E1, E1 + RGD and E2 behavior in Ringer's solution.

Table 7
Results of the electrochemical impedance spectra fitting for the PEO coatings E1, E2 and E1 + RGD tested in Ringer's solution.

Sample code	R_2 (Ω cm^2)	R_3 (Ω cm^2)	CPE1-Q ($\mu F^{n-1} \cdot cm^{-2}$)	CPE1-n	Wo-R (Ω cm^2)	Wo-T (s)	Wo-P	CPE2-Q ($\mu F^{n-1} \cdot cm^{-2}$)	CPE2-n
Ti	$2.37 \cdot 10^5 \pm 3355$	–	$6.20 \cdot 10^{-5} \pm 1.39 \cdot 10^{-7}$	0.77 ± 0.001	–	–	–	–	–
E1	4357 ± 201	–	$4.63 \cdot 10^{-6} \pm 1.47 \cdot 10^{-7}$	0.66 ± 0.003	$26{,}579 \pm 554$	0.53 ± 0.02	0.41 ± 0.002	–	–
E2	$12{,}566 \pm 557$	–	$2.14 \cdot 10^{-6} \pm 3.29 \cdot 10^{-8}$	0.78 ± 0.002	$21{,}453 \pm 1597$	0.12 ± 0.01	0.38 ± 0.001	–	–
E1 + RGD	2361 ± 37	64791 ± 2037	$5.04 \cdot 10^{-6} \pm 2.10 \cdot 10^{-7}$	0.64 ± 0.004	–	–	–	$8.07 \cdot 10^{-5} \pm 7.21 \cdot 10^{-7}$	0.66 ± 0.006

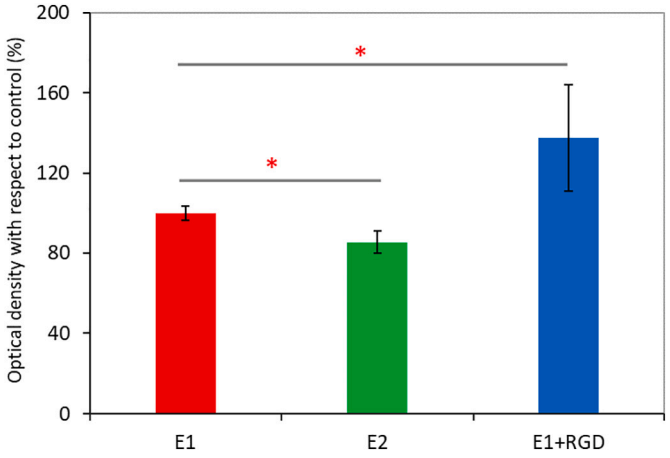

Fig. 10. Optical density for the cell proliferation from the EZ4U in vitro test using MG63 osteoblast line for the PEO coatings E1, E2 and E1 + RGD. Asterisks show the significant differences ($p < 0.05$).

proliferation of osteoblast-like MG-63 cells by about 15% over seven days on the surface of sample E2 compared to sample E1. The presence of HA did not have the expected beneficial effect on cell growth. One of the reasons may be in the surface morphology. A larger average pore size of the E1 coating may be more favorable than that of E2. Also, a decrease in the proportion of the anatase compared to the rutile could have a negative effect. The E1 + RGD sample based on β-alanine bisphosphonate with a short BMPS linker shows the best adhesion of the osteoblast-like cells. The bioactivity of the E1 + RGD sample is 37% higher compared to E1. The tests show that the modification of the PEO coating with inorganic components does not increase the surface biocompatibility. The application of the organic layer over the PEO coating significantly increases cell proliferation; this makes the proposed combination the most promising way to increase the biological activity of the surface of titanium implants.

4. Conclusions

This study has compared inorganic and organic ways to improve the bioactivity of the oxide ceramic PEO coating on titanium implants. It was shown that titania coating E1 predominantly consisting of anatase can be formed on Cp-Ti via pulsed bipolar PEO process in sodium phosphate electrolyte. Calcium-phosphate coating E2 can be formed in the same PEO regime in the electrolyte additionally containing calcium acetate; this coating contains not only titania but also hydroxyapatite and perovskite. Compared to E1, the E2 coating is thicker, it has a lower average pore size, but higher porosity and surface roughness. Also, E2 coating has lower adhesion strength and smaller coefficient of friction due to the presence of perovskite and hydroxyapatite which are softer than the rutile and anatase. The coating E1 modified with the RGD-tripeptide via a phosphonate linker shows different behavior in the XPS and EIS tests justifying the presence of the organic pore filler introduced at low acting concentrations (10^{-3} M). As follows from the EIS, the presence of the RGD peptide changes the PEO coating corrosion mechanism from diffusion-controlled to kinetic controlled. The coating E1 + RGD exhibits a 37% increase in the MG-63 cell proliferation compared to E1, whereas coating E2 shows a 15% decrease in their proliferation. Therefore, the organic trend of the PEO coating modifications seems to be preferable in the improvement of the biocompatibility of the future titanium implants.

CRediT authorship contribution statement

Evgeny Parfenov: Methodology, Writing - review & editing. **Lyudmila Parfenova:** Conceptualization, Writing - review & editing.

Veta Mukaeva: Investigation, Writing - original draft. **Ruzil Farrakhov:** Investigation, Writing - original draft. **Andrey Stotskiy:** Investigation, Visualization. **Arseniy Raab:** Investigation, Resources. **Ksenia Danilko:** Investigation, Writing - original draft. **Rameshbabu Nagumothu:** Methodology, Investigation. **Ruslan Valiev:** Supervision.

Declaration of competing interest

The authors declare that they have no known competing financial interests or personal relationships that could have appeared to influence the work reported in this paper.

Acknowledgments

This research was performed with the financial support received through the Indo-Russian joint project funded by the Russian Science Foundation, Russia (Project No. 19-49-02003), and the Department of Science and Technology, Ministry of Science and Technology, India (Project No. DST/INT/RUS/RSF/P-35). The characterization of the PEO coatings was performed at “Nanotech” Collective Usage Center of Ufa State Aviation Technical University (Russia), and at the National Institute of Technology, Tiruchirappalli (India), and this support is acknowledged with thanks. The results in synthesis and structure characterization of the RGD components were obtained on unique equipment at the “Agidel” Collective Usage Center (Ufa Federal Research Center, Russian Academy of Sciences) under the Federal Program No. AAAA-A19-119022290012-3, and with the financial support of the Ministry of Science and Higher Education of the Russian Federation (project no. 2019-05-595-000-058).

Appendix A. Supplementary data

Supplementary data to this article can be found online at https://doi.org/10.1016/j.surfcoat.2020.126486.

References

[1] M. Geetha, A.K. Singh, R. Asokamani, A.K. Gogia, Ti based biomaterials, the ultimate choice for orthopaedic implants – a review, Prog. Mater. Sci. 54 (2009) 397–425.
[2] Y. Mu, T. Kobayashi, M. Sumita, A. Yamamoto, T. Hanawa, Metal ion release from titanium with active oxygen species generated by rat macrophages in vitro, J. Biomed. Mater. Res. 49 (2000) 238–243.
[3] A. Santos-Coquillat, E. Martínez-Campos, M. Mohedano, R. Martínez-Corriá, V. Ramos, R. Arrabal, E. Matykina, In vitro and in vivo evaluation of PEO-modified titanium for bone implant applications, Surf. Coat. Technol. 347 (2018) 358–368.
[4] A. Santos-Coquillat, M. Mohedano, E. Martinez-Campos, R. Arrabal, A. Pardo, E. Matykina, Bioactive multi-elemental PEO-coatings on titanium for dental implant applications, Mater. Sci. Eng. C 97 (2019) 738–752.
[5] W.K. Yeung, G.C. Reilly, A. Matthews, A. Yerokhin, In vitro biological response of plasma electrolytically oxidized and plasma-sprayed hydroxyapatite coatings on Ti-6Al-4V alloy, J Biomed Mater Res B Appl Biomater 101 (2013) 939–949.
[6] H. Sharifi, M. Aliofkhazraei, G.B. Darband, S. Shrestha, A review on adhesion strength of peo coatings by scratch test method, Surf. Rev. Lett. 25 (2018) 1830004.
[7] M. Mohedano, R. Guzman, R. Arrabal, J.L. Lõpez Lacomba, E. Matykina, Bioactive plasma electrolytic oxidation coatings - the role of the composition, microstructure, and electrochemical stability, J. Biomed. Mater. Res. B Appl. Biomater. 101 (2013) 1524–1537.
[8] M. Echeverry-Rendón, O. Galvis, R. Aguirre, S. Robledo, J.G. Castaño, F. Echeverría, Modification of titanium alloys surface properties by plasma electrolytic oxidation (PEO) and influence on biological response, J. Mater. Sci. Mater. Med. 28 (2017).
[9] K.R. Shin, Y.S. Kim, H.W. Yang, Y.G. Ko, D.H. Shin, In vitro biological response to the oxide layer in pure titanium formed at different current densities by plasma electrolytic oxidation, Appl. Surf. Sci. 314 (2014) 221–227.
[10] L.H. Li, Y.M. Kong, H.W. Kim, Y.W. Kim, H.E. Kim, S.J. Heo, J.Y. Koak, Improved biological performance of Ti implants due to surface modification by micro-arc oxidation, Biomaterials 25 (2004) 2867–2875.
[11] S. Hariprasad, M. Ashfaq, T. Arunnellaiappan, M. Harilal, N. Rameshbabu, Role of electrolyte additives on in-vitro corrosion behavior of DC plasma electrolytic oxidization coatings formed on Cp-Ti, Surf. Coat. Technol. 292 (2016) 20–29.
[12] A. Yerokhin, E.V. Parfenov, A. Matthews, In situ impedance spectroscopy of the plasma electrolytic oxidation process for deposition of Ca- and P-containing coatings on Ti, Surf. Coat. Technol. 301 (2016) 54–62.
[13] S.-Y. Park, H.-C. Choe, Functional element coatings on Ti-alloys for biomaterials by plasma electrolytic oxidation, Thin Solid Films 699 (2020) 137896.
[14] K. Lesniak-Ziolkowska, M. Smiga-Matuszowicz, A. Blacha-Grzechnik, S. Student, M. Brzychczy-Wloch, M. Krok-Borkowicz, E. Pamula, W. Simka, A. Kazek-Kesik, Antibacterial and cytocompatible coatings based on poly(adipic anhydride) for a Ti alloy surface, Bioact. Mater. 5 (2020) 709–720.
[15] H. Fakhr Nabavi, M. Aliofkhazraei, Morphology, composition and electrochemical properties of bioactive-TiO2/HA on CP-Ti and Ti6Al4V substrates fabricated by alkali treatment of hybrid plasma electrolytic oxidation process (estimation of porosity from EIS results), Surf. Coat. Technol. 375 (2019) 266–291.
[16] S.-C. Liao, C.-T. Chang, C.-Y. Chen, C.-H. Lee, W.-L. Lin, Functionalization of pure titanium MAO coatings by surface modifications for biomedical applications, Surf. Coat. Technol. 394 (2020) 125812.
[17] C.A.H. Laurindo, R.D. Torres, S.A. Mali, J.L. Gilbert, P. Soares, Incorporation of Ca and P on anodized titanium surface: effect of high current density, Mater. Sci. Eng. C 37 (2014) 223–231.
[18] H. Wang, F. Liu, X. Xiong, S. Ke, X. Zeng, P. Lin, Structure, corrosion resistance and in vitro bioactivity of Ca and P containing TiO 2 coating fabricated on NiTi alloy by plasma electrolytic oxidation, Appl. Surf. Sci. 356 (2015) 1234–1243.
[19] S.V. Dorozhkin, Calcium orthophosphate deposits: preparation, properties and biomedical applications, Mater. Sci. Eng. C Mater. Biol. Appl. 55 (2015) 272–326.
[20] X. Rao, C.L. Chu, Q. Sun, Y.Y. Zheng, Fabrication and apatite inducing ability of different porous titania structures by PEO treatment, Mater. Sci. Eng. C Mater. Biol. Appl. 66 (2016) 297–305.
[21] H.-P. Teng, C.-J. Yang, J.-F. Lin, Y.-H. Huang, F.-H. Lu, A simple method to functionalize the surface of plasma electrolytic oxidation produced TiO2 coatings for growing hydroxyapatite, Electrochim. Acta 193 (2016) 216–224.
[22] L.F. Sukhodub, L.B. Sukhodub, W. Simka, M. Kumeda, Hydroxyapatite and brushite coatings on plasma electrolytic oxidized Ti6Al4V alloys obtained by the thermal substrate deposition method, Mater. Lett. 250 (2019) 163–166.
[23] E. Ahounbar, S.M. Mousavi Khoei, H. Omidvar, Characteristics of in-situ synthesized hydroxyapatite on TiO2 ceramic via plasma electrolytic oxidation, Ceram. Int. 45 (2019) 3118–3125.
[24] S. Lederer, S. Sankaran, T. Smith, W. Fürbeth, Formation of bioactive hydroxyapatite-containing titania coatings on CP-Ti 4+ alloy generated by plasma electrolytic oxidation, Surf. Coat. Technol. 363 (2019) 66–74.
[25] Y. Gao, A. Yerokhin, A. Matthews, Deposition and evaluation of duplex hydroxyapatite and plasma electrolytic oxidation coatings on magnesium, Surf. Coat. Technol. 269 (2015) 170–182.
[26] D. Sreekanth, N. Rameshbabu, Development and characterization of MgO/hydroxyapatite composite coating on AZ31 magnesium alloy by plasma electrolytic oxidation coupled with electrophoretic deposition, Mater. Lett. 68 (2012) 439–442.
[27] S.H. Uhm, J.S. Kwon, D.H. Song, E.J. Lee, W.S. Jeong, S. Oh, K.N. Kim, E.H. Choi, K.M. Kim, Long-term antibacterial performance and bioactivity of plasma-engineered Ag-NPs/TiO2 nanotubes for bio-implants, J. Biomed. Nanotechnol. 12 (2016) 1890–1906.
[28] X. Lu, M. Mohedano, C. Blawert, E. Matykina, R. Arrabal, K.U. Kainer, M.L. Zheludkevich, Plasma electrolytic oxidation coatings with particle additions – a review, Surf. Coat. Technol. 307 (2016) 1165–1182.
[29] B. Zhang, B. Li, S. Gao, Y. Li, R. Cao, J. Cheng, R. Li, E. Wang, Y. Guo, K. Zhang, J. Liang, B. Liu, Y-doped TiO2 coating with superior bioactivity and antibacterial property prepared via plasma electrolytic oxidation, Mater. Des. 192 (2020) 108758.
[30] F. Razzi, L.E. Fratila-Apachitei, N. Fahy, Y.M. Bastiaansen-Jenniskens, I. Apachitei, E. Farrell, A.A. Zadpoor, Immunomodulation of surface biofunctionalized 3D printed porous titanium implants, Biomed. Mater. 15 (2020) 035017.
[31] K. Venkateswarlu, N. Rameshbabu, D. Sreekanth, A.C. Bose, V. Muthupandi, S. Subramanian, Fabrication and characterization of micro-arc oxidized fluoride containing titania films on Cp Ti, Ceram. Int. 39 (2013) 801–812.
[32] M. Kaseem, H.-C. Choe, Triggering the hydroxyapatite deposition on the surface of PEO-coated Ti–6Al–4V alloy via the dual incorporation of Zn and Mg ions, J. Alloys Compd. 819 (2020) 153038.
[33] A. Kazek-Kesik, M. Krok-Borkowicz, E. Pamula, W. Simka, Electrochemical and biological characterization of coatings formed on Ti-15Mo alloy by plasma electrolytic oxidation, Mater. Sci. Eng. C Mater. Biol. Appl. 43 (2014) 172–181.
[34] N.G. Plekhova, I.N. Lyapun, E.I. Drobot, D.V. Shevchuk, S.L. Sinebryukhov, D.V. Mashtalyar, S.V. Gnedenkov, Functional state of mesenchymal stem cells upon exposure to bioactive coatings on titanium alloys, Bull. Exp. Biol. Med. 169 (2020) 147–156.
[35] S.V. Gnedenkov, S.L. Sinebryukhov, A.G. Zavidnaya, V.S. Egorkin, A.V. Puz', D.V. Mashtalyar, V.I. Sergienko, A.L. Yerokhin, A. Matthews, Composite hydroxyapatite–PTFE coatings on Mg–Mn–Ce alloy for resorbable implant applications via a plasma electrolytic oxidation-based route, J. Taiwan Inst. Chem. Eng. 45 (2014) 3104–3109.
[36] Y. Chen, G. Yan, X. Wang, H. Qian, J. Yi, L. Huang, P. Liu, Bio-functionalization of micro-arc oxidized magnesium alloys via thiol-ene photochemistry, Surf. Coat. Technol. 269 (2015) 191–199.
[37] E.V. Parfenov, L.V. Parfenova, G.S. Dyakonov, K.V. Danilko, V.R. Mukaeva, R.G. Farrakhov, E.S. Lukina, R.Z. Valiev, Surface functionalization via PEO coating and RGD peptide for nanostructured titanium implants and their in vitro assessment, Surf. Coat. Technol. 357 (2019) 669–683.
[38] L.V. Parfenova, E.S. Lukina, Z.R. Galimshina, G.U. Gil'fanova, V.R. Mukaeva, R.G. Farrakhov, K.V. Danilko, G.S. Dyakonov, E.V. Parfenov, Biocompatible organic coatings based on bisphosphonic acid RGD-derivatives for PEO-modified titanium implants, Molecules 25 (2020) 229.
[39] E. Martínez Campos, A. Santos-Coquillat, B. Mingo, R. Arrabal, M. Mohedano,

A. Pardo, V. Ramos, J.L. López Lacomba, E. Matykina, Albumin loaded PEO coatings on Ti — potential as drug eluting systems, Surf. Coat. Technol. 283 (2015) 44–51.
[40] L. Huang, J. Yi, Q. Gao, X. Wang, Y. Chen, P. Liu, Carboxymethyl chitosan functionalization of CPED-treated magnesium alloy via polydopamine as intermediate layer, Surf. Coat. Technol. 258 (2014) 664–671.
[41] M.P. Neupane, I.S. Park, M.H. Lee, Surface characterization and corrosion behavior of micro-arc oxidized Ti surface modified with hydrothermal treatment and chitosan coating, Thin Solid Films 550 (2014) 268–271.
[42] Y. He, Y. Zhang, X. Shen, B. Tao, J. Liu, Z. Yuan, K. Cai, The fabrication and in vitro properties of antibacterial polydopamine-LL-37-POPC coatings on micro-arc oxidized titanium, Colloids Surf. B: Biointerfaces 170 (2018) 54–63.
[43] A. Kazek-Kesik, A. Nosol, J. Plonka, M. Smiga-Matuszowicz, S. Student, M. Brzychczy-Wloch, M. Krok-Borkowicz, E. Pamula, W. Simka, Physico-chemical and biological evaluation of doxycycline loaded into hybrid oxide-polymer layer on Ti-Mo alloy, Bioact. Mater. 5 (2020) 553–563.
[44] E. Ruoslahti, RGD and other recognition sequences for integrins, Annu. Rev. Cell Dev. Biol. 12 (1996) 697–715.
[45] B. Elmengaard, J.E. Bechtold, K. Soballe, In vivo study of the effect of RGD treatment on bone ongrowth on press-fit titanium alloy implants, Biomaterials 26 (2005) 3521–3526.
[46] C. Mas-Moruno, P. Dorfner, F. Manzenrieder, S. Neubauer, U. Reuning, R. Burgkart, H. Kessler, Behavior of primary human osteoblasts on trimmed and sandblasted Ti6Al4V surfaces functionalized with integrin αvβ3-selective cyclic RGD peptides, J. Biomed. Mater. Res. A 101A (2013) 87–97.
[47] E. Barsukov, J.R. Macdonald, Impedance Spectroscopy: Theory, Experiment, and Applications, 2nd ed., John Willey & Sons, Inc., Hoboken, 2005.
[48] J.M. Cordeiro, B.E. Nagay, A.L.R. Ribeiro, N.C. da Cruz, E.C. Rangel, L.M.G. Fais, L.G. Vaz, V.A.R. Barão, Functionalization of an experimental Ti-Nb-Zr-Ta alloy with a biomimetic coating produced by plasma electrolytic oxidation, J. Alloys Compd. 770 (2019) 1038–1048.
[49] H.N. Pantaroto, A.P. Ricomini-Filho, M.M. Bertolini, J.H. Dias da Silva, N.F. Azevedo Neto, C. Sukotjo, E.C. Rangel, V.A.R. Barão, Antibacterial photocatalytic activity of different crystalline TiO2 phases in oral multispecies biofilm, Dent. Mater. 34 (2018) e182–e195.
[50] W.S.W. Harun, R.I.M. Asri, J. Alias, F.H. Zulkifli, K. Kadirgama, S.A.C. Ghani, J.H.M. Shariffuddin, A comprehensive review of hydroxyapatite-based coatings adhesion on metallic biomaterials, Ceram. Int. 44 (2018) 1250–1268.
[51] F.o. Cardarelli, Materials Handbook: A Concise Desktop Reference, 2nd ed., Springer, London, 2008.
[52] A.V. Naumkin, A. Kraut-Vass, S.W. Gaarenstroom, C.J. Powell, NIST X-ray Photoelectron Spectroscopy Database, NIST Standard Reference Database Number 20, National Institute of Standards and Technology, Gaithersburg MD, 2000.
[53] D. Gonbeau, C. Guimon, G. Pfister-Guillouzo, A. Levasseur, G. Meunier, R. Dormoy, XPS study of thin films of titanium oxysulfides, Surf. Sci. 254 (1991) 81–89.
[54] N.J. Price, J.B. Reitz, R.J. Madix, E.I. Solomon, A synchrotron XPS study of the vanadia-titania system as a model for monolayer oxide catalysts, J. Electron Spectrosc. Relat. Phenom. 98-99 (1999) 257–266.
[55] S. Abbasi, F. Golestani-Fard, H.R. Rezaie, S.M.M. Mirhosseini, MAO-derived hydroxyapatite/TiO2 nanostructured multi-layer coatings on titanium substrate, Appl. Surf. Sci. 261 (2012) 37–42.
[56] J. Lausmaa, B. Kasemo, H. Mattsson, Surface spectroscopic characterization of titanium implant materials, Appl. Surf. Sci. 44 (1990) 133–146.
[57] V. Zoulalian, S. Zürcher, S. Tosatti, M. Textor, S. Monge, J.J. Robin, Self-assembly of poly (ethylene glycol)-poly (alkyl phosphonate) terpolymers on titanium oxide surfaces: synthesis, interface characterization, investigation of nonfouling properties, and long-term stability, Langmuir 26 (2010) 74–82.
[58] S. Kačiulis, G. Mattogno, A. Napoli, E. Bemporad, F. Ferrari, A. Montenero, G. Gnappi, Surface analysis of biocompatible coatings on titanium, J. Electron Spectrosc. Relat. Phenom. 95 (1998) 61–69.
[59] S. Ito, J. Takebe, Longitudinal observation of thin hydroxyapatite layers formed on anodic oxide titanium implants after hydrothermal treatment in a rat maxilla model, Prosthodont. Res. Pract. 7 (2008) 82–88.
[60] S. Durdu, Ö.F. Deniz, I. Kutbay, M. Usta, Characterization and formation of hydroxyapatite on Ti6Al4V coated by plasma electrolytic oxidation, J. Alloys Compd. 551 (2013) 422–429.
[61] W.-H. Song, Y.-K. Jun, Y. Han, S.-H. Hong, Biomimetic apatite coatings on micro-arc oxidized titania, Biomaterials 25 (2004) 3341–3349.
[62] T. Hanawa, M. Ota, Calcium phosphate naturally formed on titanium in electrolyte solution, Biomaterials 12 (1991) 767–774.
[63] A.R. Boyd, G.A. Burke, H. Duffy, M.L. Cairns, P. O'Hare, B.J. Meenan, Characterisation of calcium phosphate/titanium dioxide hybrid coatings, J. Mater. Sci. Mater. Med. 19 (2008) 485–498.
[64] C.A. Antônio, N.C. Cruz, E.C. Rangel, R. De Cássia Cipriano Rangel, T. Do Espirito Santo Araujo, S.F. Durrant, B.A. Más, E.A.R. Duek, Hydroxyapatite coating deposited on grade 4 titanium by plasma electrolytic oxidation, Mater. Res. 17 (2014) 1427–1433.
[65] A. Kazek-Kęsik, D. Łastówka, A. Donesz-Sikorska, G. Dercz, W. Simka, Multilayer bioactive coatings formed on the vanadium-free titanium alloys via PEO and EPD processes, J. Electrochem. Soc. 162 (2015) D589–D597.
[66] A. Rezania, R. Johnson, Anthony R. Lefkow, K.E. Healy, Bioactivation of Metal Oxide Surfaces. 1. Surface Characterization and Cell Response, (1999).
[67] T.A. Barber, L.J. Gamble, D.G. Castner, K.E. Healy, In Vitro Characterisation of Peptide-Modified p(AAm-co-EG/AAc) IPN-Coated Titanium Implants, (2006).
[68] M.-C. Durrieu, F. Guillemot, S. Pallu, C. Labrugère, B. Brouillaud, R. Bareille, J. Amédée, N. Barthe, M. Dard, C. Baquey, Cyclo-(DfKRG) Peptide Grafting Onto Ti-6Al-4V: Physical Characterization and Interest Towards Human Osteoprogenitor Cells Adhesion, (2004).
[69] P. Wang, Y. Duan, L. Zheng, One-dimensional metal phosphonates based on 6-phosphononicotinic acid: a structural and magnetic study, SCIENCE CHINA Chem. 53 (2010) 2112–2117.
[70] P. Canepa, G. Gonella, G. Pinto, V. Grachev, M. Canepa, O. Cavalleri, Anchoring of aminophosphonates on titanium oxide for biomolecular coupling, J. Phys. Chem. C 123 (2019).
[71] J. Amalric, P.H. Mutin, G. Guerrero, A. Ponche, A. Sotto, J.-P. Lavigne, Phosphonate monolayers functionalized by silver thiolate species as antibacterial nanocoatings on titanium and stainless steel, J. Mater. Chem. 19 (2009) 141–149.
[72] N. Adden, L.J. Gamble, D.G. Castner, A. Hoffmann, G. Gross, H. Menzel, Phosphonic acid monolayers for binding of bioactive molecules to titanium surfaces, Langmuir 22 (2006) 8197–8204.
[73] M. Wagstaffe, A.G. Thomas, M.J. Jackman, M. Torres-Molina, K.L. Syres, K. Handrup, An experimental investigation of the adsorption of a phosphonic acid on the anatase TiO2(101) surface, J. Phys. Chem. C 120 (2016) 1693–1700.
[74] G. Zorn, I. Gotman, E.Y. Gutmanas, R. Adadi, G. Salitra, C.N. Sukenik, Surface modification of Ti45Nb alloy with an alkylphosphonic acid self-assembled monolayer, Chem. Mater. 17 (2005) 4218–4226.
[75] R. Luschtinetz, J. Frenzel, T. Milek, G. Seifert, Adsorption of phosphonic acid at the TiO2 anatase (101) and rutile (110) surfaces, J. Phys. Chem. C 113 (2009) 5730–5740.
[76] I. Řehoř, V. Kubíček, J. Kotek, P. Hermann, J. Száková, I. Lukeš, Modification of nanocrystalline TiO2 with phosphonate- and bis(phosphonate)-bearing macrocyclic complexes: sorption and stability studies, Eur. J. Inorg. Chem. (1981-1989), https://doi.org/10.1002/ejic.201001100(2011).